Materials Advances

PAPER

View Article Online
View Journal | View Issue

Cite this: *Mater. Adv.*, 2023, **4**, 4812

Thienyltriazine-based porous organic polymers with nitrogen rich moieties: synthesis and gas selectivity study†

Neha Rani Kumar, *[ab] Prasenjit Das,[c] Abhijeet R. Agrawal,[a]
Sanjay Kumar Mandal *[c] and Sanjio S. Zade *[a]

Received 2nd July 2023,
Accepted 6th September 2023

DOI: 10.1039/d3ma00353a

rsc.li/materials-advances

Here, we present the synthesis of a series of thienyltriazine-containing nitrogen-rich porous organic polymers by making use of Sonogashira coupling reaction (for **TT-CBz**, **TT-BCBz** and **TT-TPA**) and $FeCl_3$-mediated polymerization (for **TT-TCBz-(a–g)**). The $FeCl_3$-mediated polymerization was performed under different reaction conditions, such as oxidative polymerization, Friedel–Crafts polymerization, and competitive oxidative/Friedel–Crafts polymerizations. Polymer **TT-TCBz-b**, synthesized at room temperature in the presence of $FeCl_3$ and $MeNO_2$, displayed the highest BET surface area of approximately 1059 $m^2\ g^{-1}$. However, the percentage of micropore volume was largest for **TT-TCBz-f** and **TT-TCBz-g**, which can be attributed to their highly cross-linked structure. All of the polymers exhibited notable thermal stability, with the TT-TCBz series polymers reaching stability as high as 580 °C. The polymers of the **TT-TCBz** series were also used for CO_2 adsorption studies. The rich heteroatom content, presence of an electron-rich carbazole unit and high micropore volume make these polymers attractive candidates for sequestration of Lewis acidic CO_2 gas. A maximum CO_2 uptake of 16.5 wt% at 263 K and 100 kPa has been observed for **TT-TCBz-g** attributed to its high surface area and high percentage of micropore volume. IAST results further revealed that in **TT-TCBz-g** the selectivity for the $CO_2:N_2$ mixture (15 : 85) is around 65.

Introduction

Porous organic polymers (POPs)[1–3] have gained wider popularity over their inorganic counterparts due to their excellent stability in addition to the possibility of tuning the skeleton. Conjugated porous polymers (CPPs)[4] are one such class of POPs with an array of applications[5–10] arising from their tunable porosity, high surface area, and robust thermal and chemical stability due to the rigid π-conjugated structure.[11,12] An important advantage of conjugated POPs is the potential to synthetically introduce a range of useful chemical functionalities into the pores *via* a wide variety of organic reactions[13] and currently, intensive research into CPPs to be used as active materials in organic electronics and optoelectronics is being done.[14] Incorporation of conjugated organic semiconductors into POPs also imparts the resulting cross-linked polymers with superior properties. With careful selection of monomers and polymerization techniques, control over a wide range of physical and chemical properties can be achieved.

The properties of POPs can be tailored by choosing an appropriate design of the polymer backbone and an innovative synthesis as desired.[15] Some important strategies to control the structure of porous polymers are (a) changing the monomer length and geometry, (b) changing the reaction conditions, (c) using the statistical copolymerization technique, and (d) template-assisted synthesis. Besides these, the incorporation of electron-rich aromatic rings and heteroatoms such as nitrogen and sulfur can significantly improve host–guest interaction of porous polymers and their performance as a porous medium for the storage of small gases.

POPs have become one of the most attractive candidates for specific gas adsorption applications such as CO_2 capture and storage. Their advantages in this field emerge from their tunable porosities, easy synthesis methods, wide array of precursors available for synthesis, high surface area, thermal stability, rigid and robust structure, and regenerability.[16] Currently, gas storage and uptake are vital for environmental reasons, as they curb CO_2 emissions from human activities like burning fossil fuels, industry and power plants, thus aiding in climate change

---

[a] *Department of Chemical Sciences and Centre for Advanced Functional Materials, Indian Institute of Science Education and Research (IISER) Kolkata, Mohanpur 741246, India. E-mail: nehakumar0926@gmail.com, sanjiozade@iiserkol.ac.in*
[b] *Department of Chemistry, Dhemaji College, Dhemaji, Assam 787057, India*
[c] *Department of Chemical Sciences, Indian Institute of Science Education and Research Mohali, Sector 81, Manauli PO, S. A. S. Nagar, Mohali, Punjab 140306, India. E-mail: sanjaymandal@iisermohali.ac.in*

† Electronic supplementary information (ESI) available. See DOI: https://doi.org/10.1039/d3ma00353a

mitigation and lessening emissions. Materials for CO_2 adsorption require high surface area, porous structure, a chemical affinity for CO_2 (like amine group), stability during storage, and recyclability. Heteroatom-rich systems have emerged as particularly compelling candidates in the endeavor to engineer materials tailored for effective CO_2 adsorption.[17]

2,4,6-Tris(thiophen-2-yl)-1,3,5-triazine is one such interesting system and possesses unique features such as a π-electron deficient 1,3,5-triazine core and three thiophenes as a π-electron rich side branch, a highly symmetrical and coplanar structure (C_{3h} symmetry), the possibility of easy functionalization of α-positions of thiophene for further extension of conjugation, *etc.*[18] Both the thiophene and triazine units can lead to different types of interaction in the resulting compounds. The presence of thiophene has been known to enhance intra- and intermolecular interactions such as van der Waals interaction, π–π stacking, weak hydrogen bonds, and S···S interactions arising due to the high polarizability of the presence of sulfur. The incorporation of thienyltriazine leads to compounds with narrow band energy gap, which means the structural and optical properties of the resulting materials can be easily tuned by altering the extent of conjugation of the groups present.[19] Carbazole-containing polymers are known to show good electroactivity and photophysical properties. Incorporation of an electron rich carbazole into the POP systems imparts them with high permanent porosity, and excellent physicochemical stability besides enhancing the interaction between the sorbate molecule and the adsorbent.[20]

Inspired by the above findings and our previous work,[15] we wanted to explore further the use of the thienyltriazine system for the synthesis of POPs with systems like carbazole. Though carbazole-containing porous systems are reported in the literature,[21] we envision that incorporating all units like triazine, thiophene and carbazole into a single POP system can result in materials with excellent gas adsorption properties because all three units individually are known to enhance host–guest interactions *via* different sorts of interactions.

Herein, we describe the synthesis of a series of thienyltriazine-based polymers (**TT-CBz**, **TT-BCBz**, **TT-TCBz-(a–g)**, **TT-TPA**) incorporating other nitrogen-rich moieties like carbazole and triphenylamine. Besides using the Sonogashira coupling reaction, an inexpensive $FeCl_3$-mediated polymerization method has also been used to synthesize triazine-carbazole-based polymers through oxidative polymerization and Friedel–Crafts polymerization. $FeCl_3$-mediated oxidative polymerization and Friedel–Crafts polymerization have garnered significant attention for the synthesis of POPs.[22] In this case, cross-linked networks with methylene linkages were obtained by Friedel–Crafts reaction with dimethoxymethane, forming a flexible framework with less visible light absorption ability. The synthesized polymers exhibit high surface area, excellent thermal stability and a porous structure. **TT-TCBz-b** and **TT-TCBz-g** demonstrated CO_2 uptake of approximately 16.5 wt% (3.76 mmol g^{-1}) at STP, along with high selectivity for carbon dioxide over nitrogen.

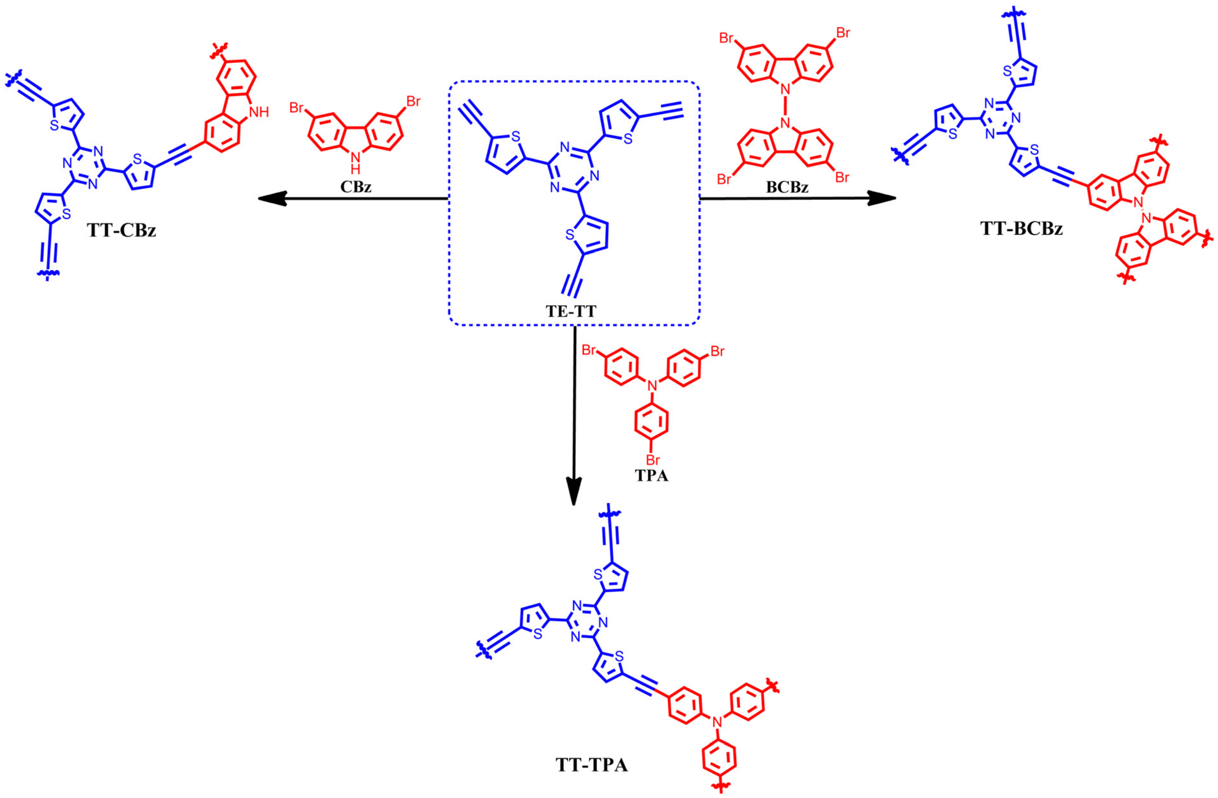

TT-CBz, TT-BCBz and TT-TPA: Synthesized by Sonogashira-Hagihara polymerisation [DMF/Et_3N (1:1), $Pd(PPh_3)_4$, CuI]

Scheme 1 Synthesis of thienyltriazine-based CPPs **TT-CBz**, **TT-BCBz** and **TT-TPA**.

Results and discussion

The synthesis of the polymers **TT-CBz**, **TT-BCBz**, **TT-TCBz-(a–g)** and **TT-TPA** was accomplished using functionalized 2,4,6-tri(thiophen-2-yl)-1,3,5-triazine and other nitrogen-containing conjugated systems. 2,4,6-Tri(thiophen-2-yl)-1,3,5-triazine was synthesized from 2-cyanothiophene using the procedure reported by Misra and their group (ESI†).[23] The synthetic route for the porous polymers is illustrated in Schemes 1 and 2. **TT-CBz**, **TT-BCBz** and **TT-TPA** were obtained through the Sonogashira coupling reaction of 2,4,6-tris(5-ethynylthiophen-2-yl)-1,3,5-triazine (**TE-TT**) with dibromocarbazole (**CBz**), tetrabromo-bicarbazole (**BCBz**) and tribromotriphenylamine (**TPA**), respectively. For the synthesis of the **TT-TCBz** polymer series, the initial step involved the synthesis of a precursor in which thienyltriazine was flanked by three carbazole units at the α-carbon of thiophene. This precursor was synthesized using a method reported in the literature for a similar compound with benzene at the core (Scheme S1, ESI†).[20] This precursor (**TT-TCBz**) was used for $FeCl_3$-mediated polymerization under different conditions: (1) oxidative polymerization (OP), (2) Friedel–Crafts polymerization (FCP), and (3) competitive oxidative/Friedel–Crafts polymerization (CO/FC-P) (Scheme 2). Under oxidative conditions, we explored five different reaction conditions by altering the reaction solvent, temperature, and presence or absence of $MeNO_2$, as shown in Scheme 2.

The successful formation of the porous polymeric backbone and the incorporation of the monomers into the framework were studied by Fourier transform infrared (FT-IR) spectroscopy (Fig. 1 and Fig. S1, S2, ESI†), solid-state ^{13}C CP/MAS NMR spectroscopy (Fig. 2), elemental analysis (Table S2, ESI†) and solid-state UV-visible absorption spectroscopy (Fig. S3a and b, ESI†). Polymers **TT-CBz**, **TT-BCBz** and **TT-TPA** feature a disubstituted C–C triple bond, confirmed by a weak band around 2180 cm^{-1} in the IR spectra. The stretching vibrations around 1500, 1370 and 800 cm^{-1} in all the polymers are characteristic of the *s*-triazine moiety. Peaks at approximately 3080 cm^{-1} and 1625 cm^{-1} are assigned to sp^2-C–H stretching and C–C double bond stretching of the thiophene ring. A peak at 3403–3450 cm^{-1} indicates the ability of porous polymers to absorb moisture from the air. A comparison of the FT-IR spectra of the precursors and the corresponding polymers is presented in Fig. S1, ESI.† In the solid-state ^{13}C NMR spectra, all the **CPPs** exhibited a peak at around 167–168 ppm, corresponding to the carbon of the triazine ring. The peaks in the range of 84–96 ppm in the solid-state ^{13}C NMR spectra of **TT-CBz**, **TT-BCBz** and **TT-TPA** correspond to quaternary alkyne carbons involved in polymerization. The peaks at around 143–148 ppm correspond to thiophene carbon bonded to the triazine ring (α carbon). Additional peaks in the range of 110–135 ppm correspond to other carbon atoms of thiophene

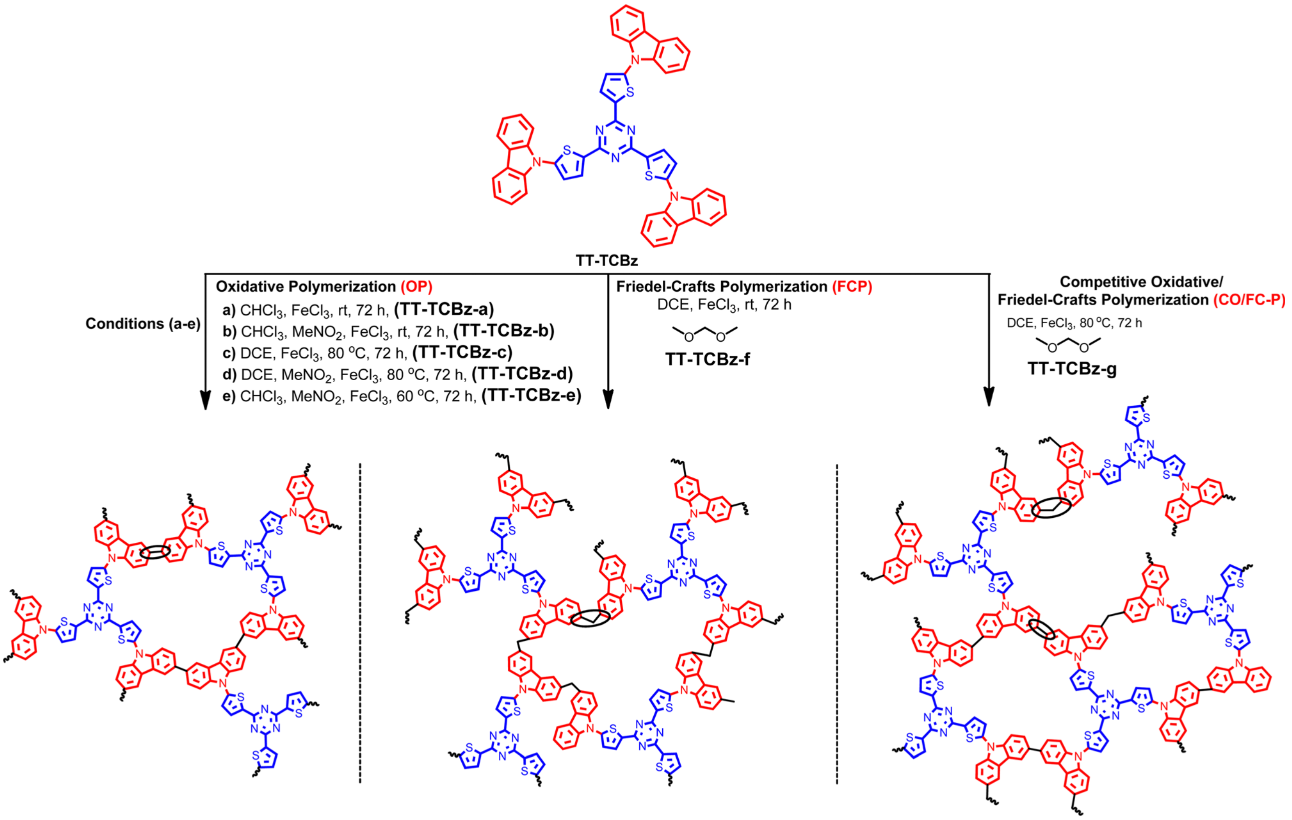

* All the reactions were done under an inert atmosphere

Scheme 2 Polymerization of **TT-TCBz** under different reaction conditions in the presence of $FeCl_3$ to give polymers **TT-TCBz-a**, **TT-TCBz-b**, **TT-TCBz-c**, **TT-TCBz-d**, **TT-TCBz-e**, **TT-TCBz-f**, and **TT-TCBz-g**, respectively.

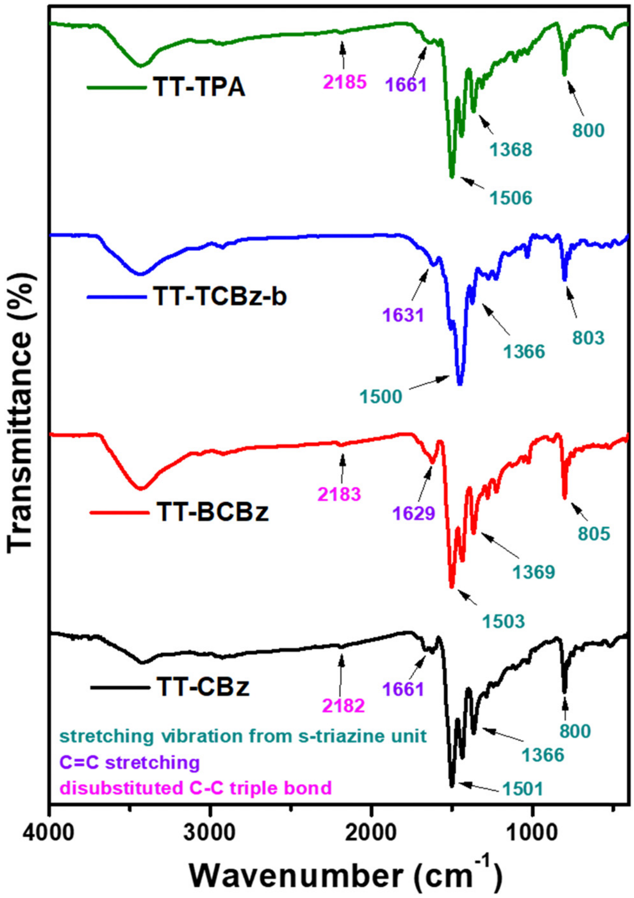

Fig. 1 Stacked FT-IR spectra of **TT-CBz**, **TT-BCBz**, **TT-TCBz-b**, and **TT-TPA**, respectively.

from thienyltriazine and the phenyl pendant of carbazole and triphenylamine.

Polymers **TT-TCBz-f** and **TT-TCBz-g** exhibited several peaks in the aliphatic region due to the Friedel–Crafts reaction between the monomer **TT-TCBz** and dimethoxymethane. Such peaks are commonly observed in Friedel–Crafts polymerization reaction (Fig. 2(E) and (F)).[24] By combining the results of FT-IR and solid-state ^{13}C NMR studies, we can conclude that the represented polymer skeletons were formed. The C, H, and N contents of the polymers were determined (Table S2, ESI†) through elemental analysis. The experimental results showed deviation from the theoretically obtained values, which can be attributed to the presence of unreacted end groups, catalyst residues, and the trapped gases and moisture from the air in the samples. All three polymers, except those in the **TT-TCBz** series, possess an extended π-conjugation, corroborated by the broad absorption profile in the solid-state UV-visible spectra with the absorption profile extending from 350 nm to 750 nm (Fig. S3a, ESI†). The hindered conjugation due to the bicarbazole unit in **TT-BCBz** is evident from its blue-shifted absorption compared to **TT-CBz** and **TT-TPA**. Polymers **TT-TCBz-(a–g)** have their absorption profile centered between 300 nm and 550 nm, which is expected from its structure having hindered conjugation created by the three carbazole units flanked on the thienyltriazine core (Fig. S3b, ESI†). The Kubelka–Munk plot was used to calculate the band gap of the polymers (Fig. S4 and S5, ESI†). Their band gap values follow the trend **TT-TPA** < **TT-CBz** < **TT-BCBz** < **TT-TCBz-b**. This trend aligns with the extent of conjugation of the polymers. The conjugation is hindered in **TT-BCBz** and **TT-TCBz-b**, resulting in their higher band gap. The band gap of the polymers **TT-TCBz (a–g)** lies in the range 2.25–2.78 eV. The band gap values of the polymers indicate the potential of these materials in optical applications.

Powder X-ray diffraction measurements (Fig. S6a and b, ESI†) reveal broad diffraction peaks, which confirm the disordered, amorphous nature of the polymers and can be attributed to the kinetic control of the reaction. Though the porous polymers were subjected to extensive Soxhlet purification and were also washed with 6N HCl, some sharp peaks were observed in the PXRD spectrum of **TT-TCBz-e** and **TT-TCBz-f** (Fig. S6b, ESI†). This might arise from the residual metal ion present in the sample due to the favorable interaction between the nitrogen atom of the polymer and iron.[25] Thermal gravimetric analysis (TGA) measurements revealed the high thermal stability of the polymers, as more than 90% of the mass is retained even at 450 °C for polymers **TT-CBz**, **TT-BCBz**, and **TT-TPA**. **TT-TCBz-a**, **TT-TCBz-b**, **TT-TCBz-d** and **TT-TCBz-e** are among the most thermally stable polymers reported, with their decomposition temperature around 590 °C (Fig. S7a and b, ESI†).

The morphology of the polymers was examined using transmission electron microscopy (TEM) and scanning electron microscopy (SEM) (Fig. 3 and Fig. S8, ESI†). Except for the polymer **TT-BCBz**, which exhibits a morphology consisting of small fibres (Fig. 3(d)–(f)), all other polymers (**TT-CBz, TT-TCBz-(a–g)**, **TT-TPA**) have a very similar small particle-like morphology, as evidenced by their respective TEM images. However, this particle size was uniform only in **TT-TCBz-a, TT-TCBz-b, TT-TCBz-d** and **TT-TPA**. All the other polymers displayed a morphology comprising particles of varied sizes.

The permanent porosity (*i.e.*, polymer surface area) and the pore size distributions of the polymers were measured through nitrogen adsorption and desorption at 77.3 K. Insight into the porous properties revealed that all the polymers exhibit a mixture of Type II and Type IV adsorption isotherms (Fig. 4(A) and (B)) according to IUPAC classification. The polymers **TT-CBz, TT-BCBz,** and **TT-TPA** display a sharp increase in N_2 uptake at $P/P_0 = 0.9–1$, suggesting the dominance of meso- and macropores from the inter-particle voids in these polymers. The uptake of N_2 at relatively low pressures $P/P_0 < 0.1$ is very low, indicating relatively low microporosity in these polymers (Fig. 4(A)). However, the polymers **TT-TCBz (a–g)** display a reasonable increase in N_2 uptake at relatively low pressures $P/P_0 < 0.1$, indicating the absence of macropores and dominance of micro and mesopores (Fig. 4(B)). Moreover, all the polymers show an open-loop behavior in the desorption cycle, indicating their ability to undergo expansion. **TT-TCBz-b** exhibits excellent swelling ability on the addition of solvents like methanol or THF to the dried polymer. As depicted in Table 1, the BET surface area was found to be 13, 316, 1059 and 54 m^2 g^{-1} for **TT-CBz, TT-BCBz, TT-TCBz-b**, and **TT-TPA**, respectively. The high surface area of **TT-TCBz-b**

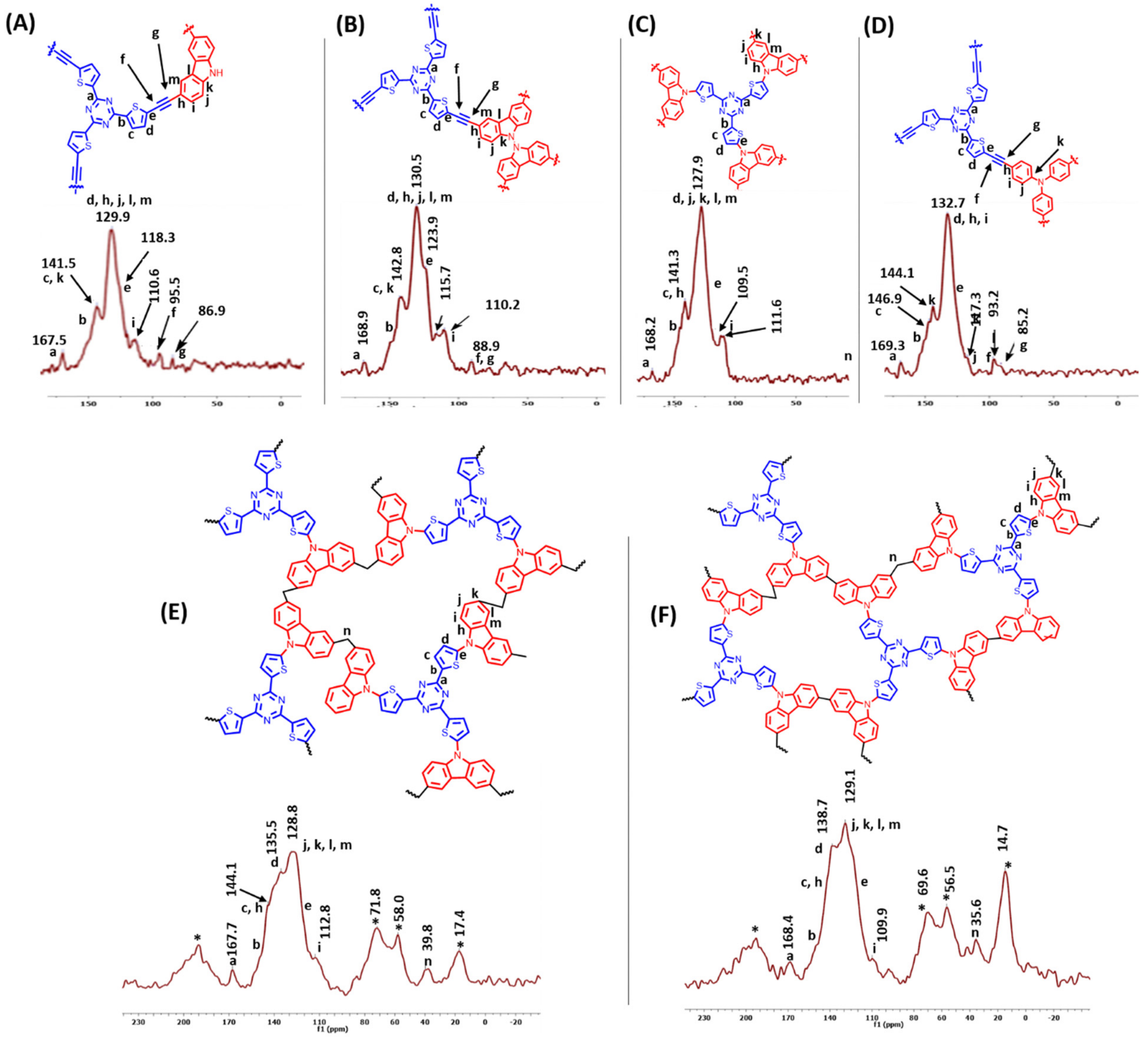

Fig. 2 Fig. 2 Solid-state 13C NMR spectra of (A) TT-CBz, (B) TT-BCBz, (C) TT-TCBz-b, (D) TT-TPA, (E) TT-TCBz-f and (F) TT-TCBz-g, respectively (* The peaks marked by asterisks represent the spinning sidebands).

compared to other polymers can be attributed to the facile $FeCl_3$-mediated polymerization of the carbazole units. The pore diameter of the polymers was determined by the Barrett–Joyner–Halenda method.[26] With the exception of **TT-TCBz-b**, the other polymers primarily exhibit a major distribution of pores within the macropore range (Fig. 5(A)). All the polymers in the **TT-TCBz** series had a very narrow pore size distribution of around 3.2–4.1 nm (Fig. 5(B)). However, the expected general trend that an increase in temperature leads to an increase in surface area was not observed in these polymers. Inagaki and co-workers reported the synthesis of spirobifluorene-based polymers synthesized by oxidative polymerization, Friedel–Crafts polymerization and competitive oxidative and Friedel–Crafts polymerization.[27] The trend observed for the BET surface area in the present study is different from the one observed by Inagaki and their group on the spirobifluorene system.

We synthesized the polymer of precursor **TT-TCBz** under seven different conditions, among which **TT-TCBz-b** displayed the best surface area of 1054 $m^2\ g^{-1}$. However, both cross-linked polymers, **TT-TCBz-f** and **TT-TCBz-g** exhibit high micropore surface area and a high percentage of micropore volume. The significant increase in surface area upon using $MeNO_2$ along with $FeCl_3$ can be attributed to the enhanced solubility of $FeCl_3$, which aids in the polymerization reaction.

Porous materials with a high surface area are known to show high CO_2 adsorption capacity. However, increasing the heteroatom content of the polymer and incorporating functionalities capable of generating an electrostatic field on the porous surface are highly desirable to enhance the interaction of CO_2 with the porous medium. Porous polymers rich in heteroatom content are recognized for their ability to facilitate dipole–quadrupole interaction, which in turn increases the affinity of

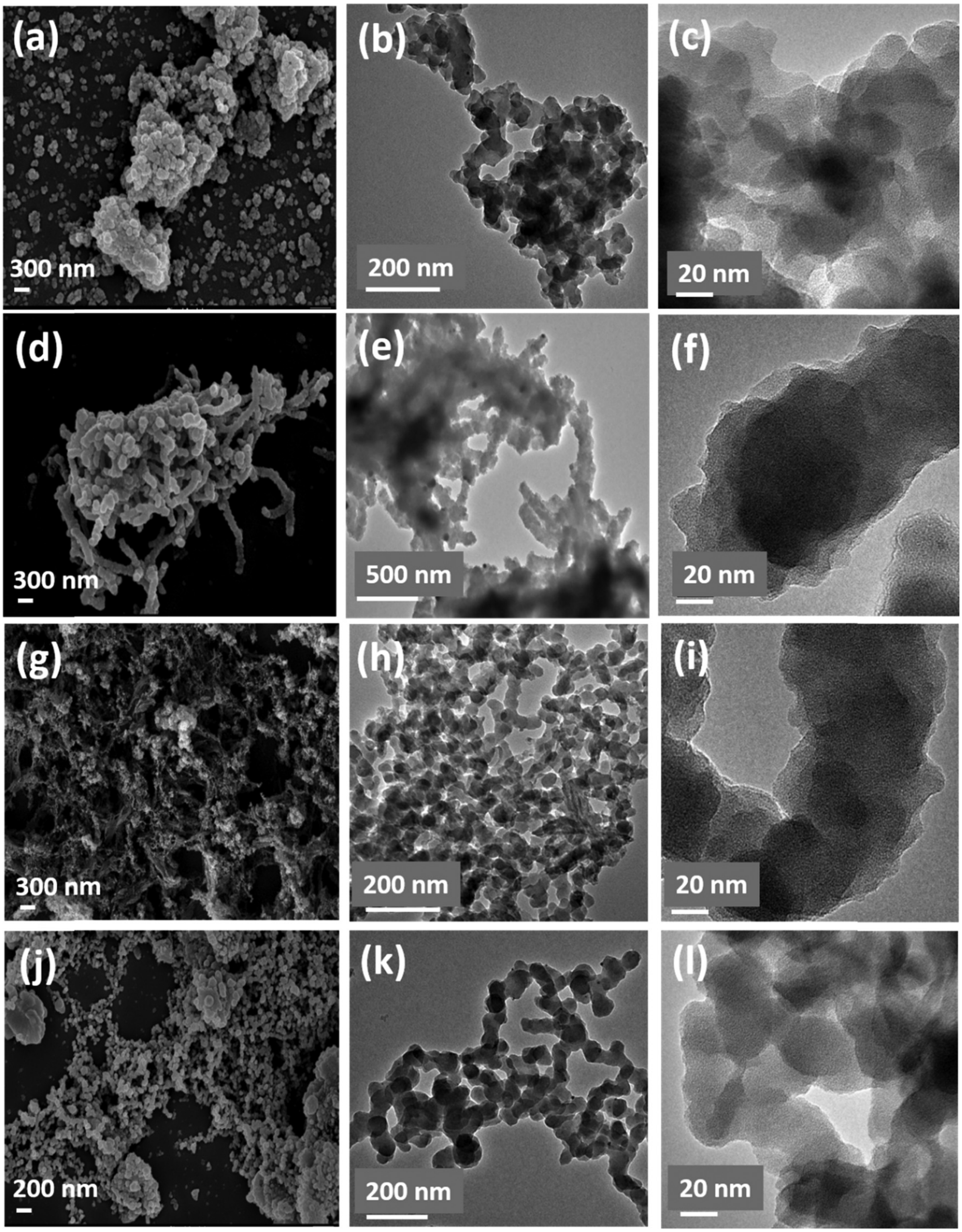

Fig. 3 SEM images of (a) **TT-**, (d) **TT-BCBz**, (g) **TT-TCBz-b** and (j) **TT-TPA**; TEM images of (b) **TT-CBz,** (e) **TT-BCBz,** (h) **TT-TCBz-b** and (k) **TT-TPA**; HRTEM images of (c) **TT-CBz,** (f) **TT-BCBz,** (i) **TT-TCBz-b** and (l) **TT-TPA**, respectively.

CO_2 towards the porous material.[28] The electron-rich nature of carbazoles has made polycarbazoles a potential material for CO_2 sequestration.[29] The polymers belonging to the **TT-TCBz** series have the added benefits of three carbazole units flanked on the thienyltriazine system, making them highly potential candidates to be explored in CO_2 adsorption and gas selectivity studies. Besides that, all the polymers in the **TT-TCBz** series also had high BET surface area compared to the other three polymers. We evaluated the polymers **TT-TCBz-(a–g)** for their affinity to adsorb CO_2 using BET sorption analysis. Fig. 6 and Table 2 show the CO_2 adsorption isotherms of the porous copolymer, **TT-TCBz-a**, **TT-TCBz-b**, **TT-TCBz-c**, **TT-TCBz-d**, **TT-TCBz-e**, **TT-TCBz-f,** and **TT-TCBz-g** at 263 K, 273 K and 298 K. In all cases it can be seen that CO_2 uptake capacity increases

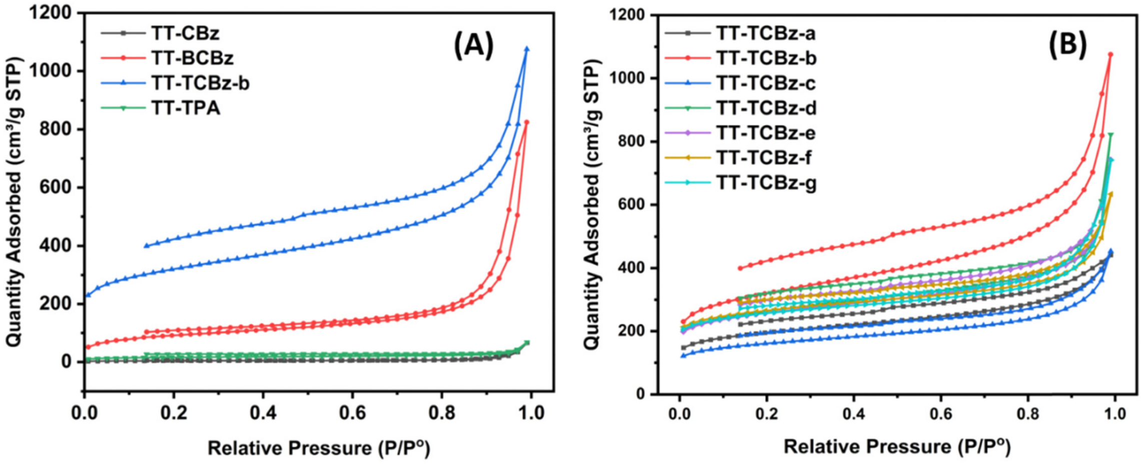

Fig. 4 (A) Stacked N_2 adsorption–desorption isotherms of **TT-CBz**, **TT-BCBz**, **TT-TCBz-b** and **TT-TPA.** (B) Stacked N_2 adsorption–desorption isotherms of **TT-TCBz-a**, **TT-TCBz-b**, **TT-TCBz-c**, **TT-TCBz-d**, **TT-TCBz-e**, **TT-TCBz-f**, and **TT-TCBz-g**, respectively.

Table 1 Porosity parameters of the CPPs **TT-CBz**, **TT-BCBz**, **TT-TCBz-b**, and **TT-TPA**

Sample code	S_{BET} [m^2 g^{-1}]	S_{Micro}[b] [m^2 g^{-1}]	S_{Langmuir} [m^2 g^{-1}]	Average pore diameter (nm)	V_{Micro} [cm^3 g^{-1}]	V_{Total} [cm^3 g^{-1}]	$S_{\mathrm{Micro/BET}}$ (%)	$V_{\mathrm{Micro}}/V_{\mathrm{Total}}$ (%)
TT-CBz	13	6	23	2.7	0.003100	0.004319	46	71
TT-BCBz	316	49	641	7	0.025264	0.560830	15	4.5
TT-TCBz-b	1059	401	1980	4	0.207263	1.093440	38	18.9
TT-TPA	54	19	95	3.5	0.009832	0.048306	35	20

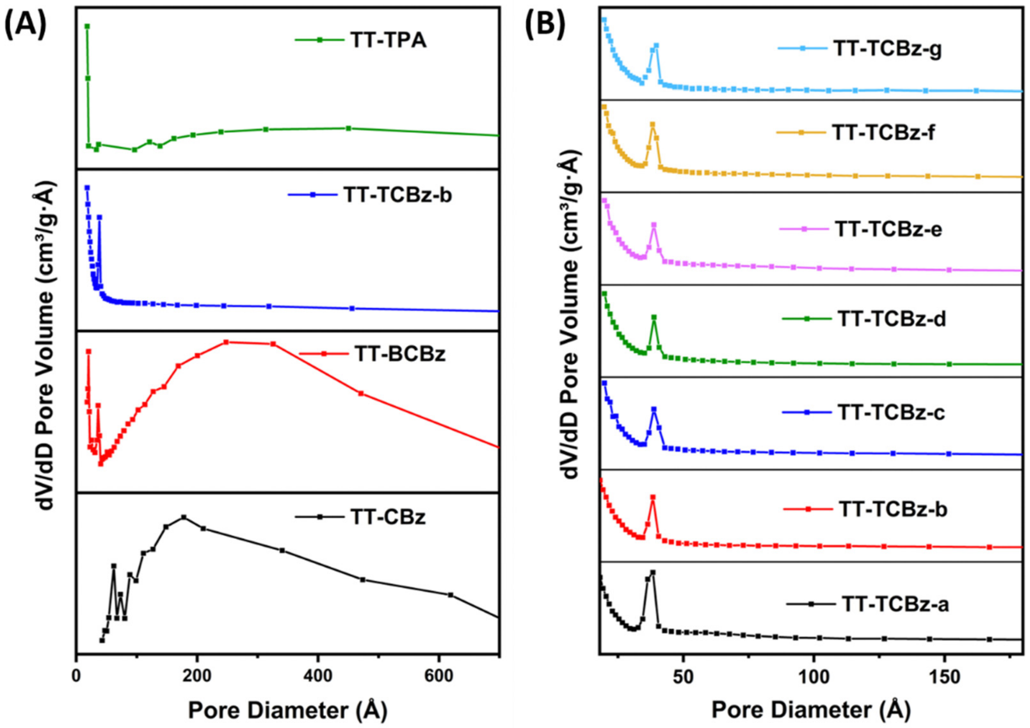

Fig. 5 (A) Pore-size distribution curves of **TT-CBz**, **TT-BCBz**, **TT-TCBz-b** and **TT-TPA.** (B) Pore-size distribution curves of **TT-TCBz-a**, **TT-TCBz-b**, **TT-TCBz-c**, **TT-TCBz-d**, **TT-TCBz-e**, **TT-TCBz-f**, and **TT-TCBz-g**, respectively.

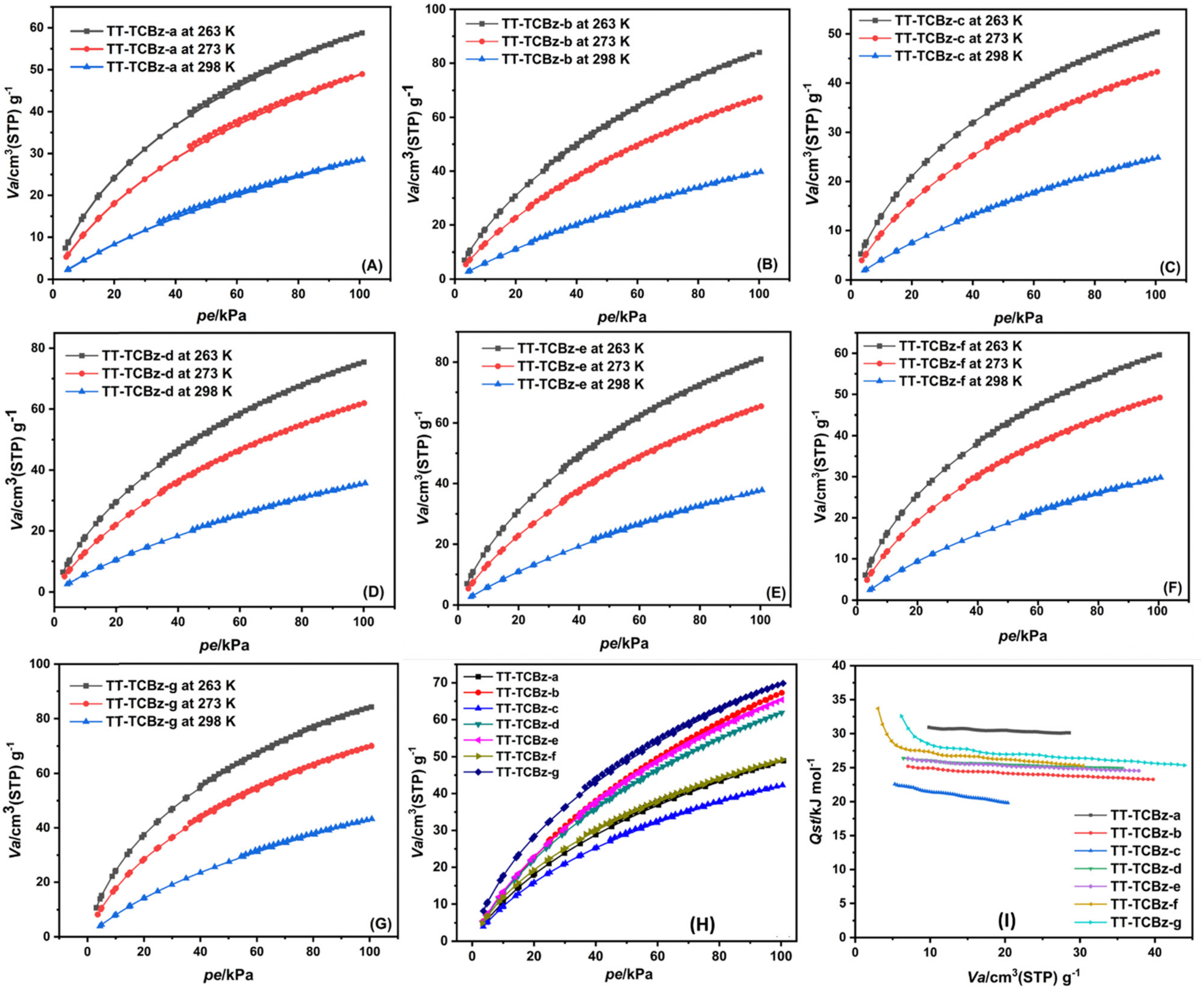

Fig. 6 CO_2 adsorption–desorption isotherms of (A) **TT-TCBz-a**, (B) **TT-TCBz-b**, (C) **TT-TCBz-c**, (D) **TT-TCBz-d**, (E) **TT-TCBz-e**, (F) **TT-TCBz-f**, (G) **TT-TCBz-g** at different temperatures, respectively; (H) CO_2 adsorption–desorption isotherms of **TT-TCBz-a**, **TT-TCBz-b**, **TT-TCBz-c**, **TT-TCBz-d**, **TT-TCBz-e**, **TT-TCBz-f**, and **TT-TCBz-g** at 273 K, respectively and (I) isosteric heat of adsorption of CO_2 gas on **TT-TCBz-a**, **TT-TCBz-b**, **TT-TCBz-c**, **TT-TCBz-d**, **TT-TCBz-e**, **TT-TCBz-f**, and **TT-TCBz-g**, respectively.

monotonically with increasing CO_2 pressure. The CO_2 adsorption capacity of the material is calculated as 11.4 wt% (2.6 mmol g^{-1}), 16.5 wt% (3.75 mmol g^{-1}), 9.8 wt% (2.24 mmol g^{-1}), 14.7 wt% (3.36 mmol g^{-1}), 15.8 wt% (3.61 mmol g^{-1}), 11.70 wt% (2.66 mmol g^{-1}), and 16.58 wt% (3.77 mmol g^{-1}) at 263.0 K/100 kPa for **TT-TCBz-a**, **TT-TCBz-b**, **TT-TCBz-c**, **TT-TCBz-d**, **TT-TCBz-e**, **TT-TCBz-f**, and **TT-TCBz-g**, respectively. The high CO_2 adsorption capacity of the polymers can be attributed to the rich heteroatom content (N and S) that leads to increased dipole–quadrupole interactions between the polymer skeleton and CO_2 molecule. We had also given theoretical evidence of the interaction of both N and S of thienyltriazine with CO_2 molecules in our earlier report.[15] Also, the electron-rich carbazole in the polymer framework and high charge density at the nitrogen site can enhance the interaction of POPs with the polarisable CO_2 molecules. The CO_2 adsorption is lowest for **TT-TCBz-c**, which also has the lowest BET surface area. **TT-TCBz-b** and **TT-TCBz-g** show the highest CO_2 adsorption but almost equal capacity. The high adsorption capacity of **TT-TCBz-b** is a consequence of its high BET surface area, whereas for polymer **TT-TCBz-g** the high CO_2 adsorption capacity, despite having a BET surface area comparable to other polymers, can be a direct consequence of its cross-linked structure and high percentage of micropore volume. The reversible natures of these isotherms indicated the absence of chemisorption of CO_2 over **TT-TCBz-(a–g)**. The isosteric heat of adsorption (Qst) is calculated from the CO_2 isotherms measured at 263, 273, and 298 K temperatures by using the Clausius–Clapeyron equation. The isosteric heats of adsorption are plotted as a function of the amount of CO_2 uptake in Fig. 6(I). These Qst values are below the energy of the chemical bond formation, but quite high heat of adsorption due to the presence of triazine rings suggested the strong interaction of CO_2 molecules at the surface of the copolymers. **TT-TCBz-b** and

Table 2 Porosity parameters of the polymers **TT-TCBz-a**, **TT-TCBz-b**, **TT-TCBz-c**, **TT-TCBz-d**, **TT-TCBz-e**, **TT-TCBz-f**, and **TT-TCBz-g**, respectively

Sample code	S_{BET}[a] [$m^2\ g^{-1}$]	S_{Micro}[b] [$m^2\ g^{-1}$]	$S_{Langmuir}$ [$m^2\ g^{-1}$]	Average pore diameter (nm)	V_{Micro}[c] [$cm^3\ g^{-1}$]	V_{Total}[d] [$cm^3\ g^{-1}$]	$S_{Micro/BET}$ (%)	V_{Micro}/V_{Total} (%)	CO_2 uptake (mmol g^{-1}) at 100 kPa		
									263 K	273 K	298 K
TT-TCBz-a	637	285	1152	3.5	0.147921	0.569	44	25.97	2.61	2.21	1.29
TT-TCBz-b	1059	401	1980	4	0.207263	1.093	38	18.9	3.75	3.00	1.77
TT-TCBz-c	523	227	95 662	3.4	0.118968	0.189	43.4	62.9	2.24	1.88	1.10
TT-TCBz-d	854	391	1533	3.7	0.204468	0.314	45.7	65.07	3.36	2.76	1.58
TT-TCBz-e	832	404	1479	3.7	0.210460	0.309	48.5	68.1	3.61	2.91	1.68
TT-TCBz-f	821	474	1439	4.1	0.245843	0.332	57.7	74.7	2.66	2.19	1.33
TT-TCBz-g	848	465	1390	4.1	0.241056	0.321	54.8	75.1	3.77	3.11	1.92

[a] S_{BET} is the surface area calculated from the N_2 adsorption isotherm in the relative pressure (P/P_0) range. [b] S_{Micro} is the microporous surface area calculated from the N_2 adsorption isotherm based on the Harkins Jura method. [c] V_{Micro} is the microporous volume derived from the *t* plot. [d] V_{Total} is the total pore volume at $P/P_0 = 0.996$.

TT-TCBz-g with surface area of 1059 $m^2\ g^{-1}$ and 848 $m^2\ g^{-1}$, respectively, show a decent CO_2 adsorption of 3.00 mmol g^{-1} and 3.11 mmol g^{-1} at 273 K and 1 bar if compared to the CO_2 adsorption of some POPs synthesized using similar conditions and having high surface area such as COP-3[23] (S_{BET} = 1980 $m^2\ g^{-1}$, CO_2 adsorption: 4.6 mmol g^{-1} at 273 K and 1 bar), COP-3-rt[23] (S_{BET} = 1490 $m^2\ g^{-1}$, CO_2 adsorption: 3.5 mmol g^{-1} at 273 K and 1 bar), CPOP-1[18] (S_{BET} = 2220 $m^2\ g^{-1}$, CO_2 adsorption: 4.8 mmol g^{-1} at 273 K and 1 bar) and CNOP-2[19e] (S_{BET} = 1546 $m^2\ g^{-1}$, CO_2 adsorption: 4.0 mmol g^{-1} at 273 K and 1 bar). The adsorption capacity of the POPs reported here is comparable and even higher in some cases compared to some POPs reported in the literature with a very high surface area (Table S3, ESI†).

Considering the high surface area as well as the high CO_2 adsorption of **TT-TCBz-b** and **TT-TCBz-g**, we conducted selectivity calculations for $CO_2:N_2$ with an increasing CO_2 mol% from 5 to 25% at an interval of 5% mixture of CO_2/N_2 at 298 K. We utilized the ideal adsorbed solution theory (IAST), as developed by Myers and Prausnitz for binary mixtures at a pressure of 1 bar.[30] The mixture composition $CO_2:N_2$ (15:85) holds particular significance, being representative of flue gas composition and the separation of CO_2 from N_2 during the post-combustion process is crucial. It is clear from the gas uptake

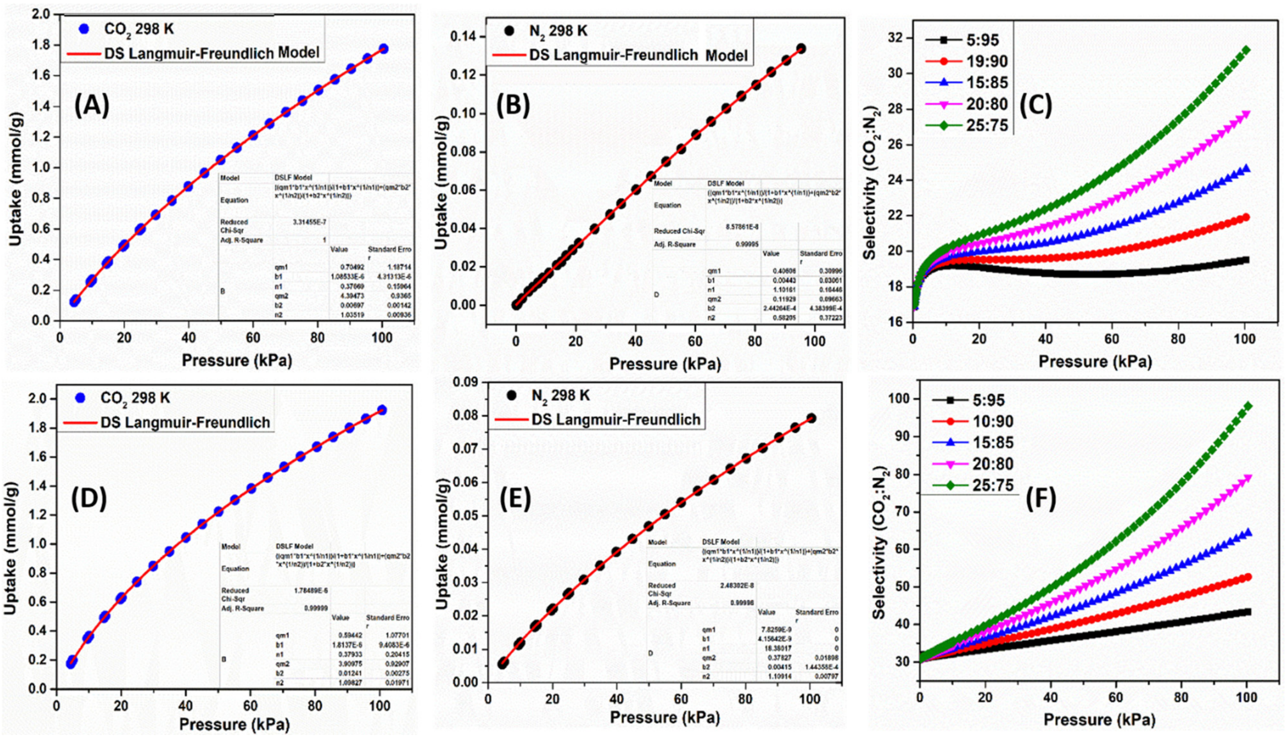

Fig. 7 (A) and (D) Dual-site Langmuir–Freundlich fitting (a) (red line) for the CO_2 (blue cycle) isotherm measured at 298 K for **TT-TCBz-b** and **TT-TCBz-g**, respectively. (B) and (E) Dual site Langmuir–Freundlich fitting (a) (red line) for the N_2 (black cycle) isotherm measured at 298 K for **TT-TCBz-b** and **TT-TCBz-g**, respectively. (C) and (F) Selectivity of CO_2 over N_2 at 298 K: change of adsorption selectivity with increasing CO_2 mol% from 5 to 25% at an interval of 5% mixture of CO_2/N_2 for **TT-TCBz-b** and **TT-TCBz-g,** respectively.

curves that CO_2 uptake is high compared to that of N_2 at 298 K (Fig. 7(A), (B), (D) and (E)). This can be a consequence of the quadrupole moment and kinetic diameter difference between these gases (CO_2, 3.30 Å; N_2, 3.64 Å) that allows easy diffusion of CO_2 molecules into the pores.[31] The uptake behavior of CO_2 and N_2 gases at 298 K for **TT-TCBz-b** and **TT-TCBz-g** have been fitted using the dual-site Langmuir–Freundlich model (DS-LF) (Fig. 7(A) (B), (D) and (E)). Furthermore, the IAST results indicate that for **TT-TCBz-b** the selectivity for the $CO_2:N_2$ (15 : 85) mixture is 24.5 (Fig. 7(C)) at 298 K, whereas for **TT-TCBz-g**, it is approximately 65 (Fig. 7(F)). Despite having the same pore size, this disparity can be attributed to the cross-linked structure and the notably higher percentage of micropore volume in **TT-TCBz-g**. The selectivity displayed by **TT-TCBz-g** for CO_2 over N_2 at ambient conditions is comparable and even higher than several POPs reported in the literature (Table S4, ESI†).[28c]

Conclusion

In summary, we have reported the synthesis and properties of heteroatom-rich polymers containing thienyltriazine and other nitrogen-rich moieties. The main focus of this work was an inexpensive $FeCl_3$-mediated method for the synthesis of triazine-carbazole-based polymers through oxidative polymerization, Friedel–Crafts polymerization and competitive oxidative/Friedel–Crafts polymerization. Furthermore, in addition to exhibiting a high BET surface area, the cross-linked flexible polymers showed high thermal stability, and CO_2 uptake, reaching as high as 16.5 wt% at 263 K and 1 atm. The polymers also displayed high CO_2 selectivity over nitrogen. In particular, the high CO_2 selectivity of **TT-TCBz-g** over N_2 can be attributed to its cross-linked structure and a high percentage of micropore volume. These polymers can be potential materials for further exploration into CO_2 trapping and conversion reactions. Overall, their potential as organic semiconductors for energy and environmental applications form the basis for future studies.

Conflicts of interest

There are no conflicts to declare.

Acknowledgements

S. K. M. acknowledges IISER Mohali for funding. N. R. K. thanks DST for an INSPIRE fellowship. A. R. A. thanks IISER Kolkata for a fellowship. We also acknowledge TEM, DST-FIST facility, IISER Kolkata, JEM-2100F. SERB, India is acknowledged for funding (CRG/2018/002784).

References

1 S. Xu, Y. Luo and B. Tan, *Macromol. Rapid Commun.*, 2013, **34**, 471–484.

2 C. Y. Gu, D. Y. Liu, W. Huang, J. Liu and Q. R. Yang, *Polym. Chem.*, 2015, **6**, 7410–7417.

3 (*a*) H. Cheng, T. Hasell, A. Trewin, D. J. Adams and A. I. Cooper, *Angew. Chem. Int. Ed.*, 2012, **51**, 12727–12731; (*b*) A. I. Cooper, *Adv. Mater.*, 2009, **21**, 1291–1295; (*c*) S. Ren, M. J. Bojdys, R. Dawson, A. Laybourn, Y. Z. Khimyak, D. J. Adams and A. I. Cooper, *Adv. Mater.*, 2012, **24**, 2357–2361.

4 Y. Xu, S. Jin, H. Xu, A. Nagai and D. Jiang, *Chem. Soc. Rev.*, 2013, **42**, 8012–8031.

5 (*a*) C. D. Wood, B. Tan, A. Trewin, H. J. Niu, D. Bradshaw, M. J. Rosseinsky, Y. Z. Khimyak, N. L. Campbell, R. Kirk, E. Stockel and A. I. Cooper, *Chem. Mater.*, 2007, **19**, 2034–2048; (*b*) J. X. Jiang, F. Su, H. Niu, C. D. Wood, N. L. Campbell, Y. Z. Khimyak and A. I. Cooper, *Chem. Commun.*, 2008, 486–488; (*c*) C. D. Wood, B. Tan, A. Trewin, F. Su, M. J. Rosseinsky, D. Bradshaw, Y. Sun, L. Zhou and A. I. Cooper, *Adv. Mater.*, 2008, **20**, 1916–1921; (*d*) R. Dawson, D. J. Adams and A. I. Cooper, *Chem. Sci.*, 2011, **2**, 1173–1177; (*e*) P. M. Budd, A. Butler, J. Selbie, K. Mahmood, B. McKeown, K. Ghanem, D. Book and A. Walton, *Phys. Chem. Chem. Phys.*, 2007, **9**, 1802–1808; (*f*) N. B. McKeown, P. M. Budd and D. Book, *Macromol. Rapid Commun.*, 2007, **28**, 995–1002; (*g*) A. Li, R. F. Lu, Y. Wang, X. Wang, K. L. Han and W. Q. Deng, *Angew. Chem. Int. Ed.*, 2010, **49**, 3330–3333.

6 (*a*) X. Wang, K. Maeda, A. Thomas, K. Takanabe, G. Xin, J. M. Carlsson, K. Domen. and M. A. Antonietti, *Nat. Mater.*, 2009, **8**, 76–80; (*b*) X. Wang, K. Maeda, X. Chen, K. Takanabe, K. Domen, Y. Hou, X. Fu and M. Antonietti, *J. Am. Chem. Soc.*, 2009, **131**, 1680–1681; (*c*) M. G. Schwab, M. Hamburger, X. Feng, J. Shu, H. W. Spiess, X. Wang, M. Antonietti and K. Mullen, *Chem. Commun.*, 2010, **46**, 8932–8934.

7 (*a*) F. Goettmann, A. Fischer, M. Antonietti and A. Thomas, *Angew. Chem. Int. Ed.*, 2006, **45**, 4467–4471; (*b*) X. Wang, K. Maeda, X. Chen, K. Takanabe, K. Domen, Y. Hou, X. Fu and M. Antonietti, *J. Am. Chem. Soc.*, 2009, **131**, 1680–1681; (*c*) J. X. Jiang, C. Wang, A. Laybourn, T. Hasell, R. Clowes, Y. Z. Khimyak, J. Xiao, S. J. Higgins, D. J. Adams and A. I. Cooper, *Angew. Chem., Int. Ed.*, 2011, **50**, 1072–1075; (*d*) L. Chen, Y. Yang and D. Jiang, *J. Am. Chem. Soc.*, 2010, **132**, 9138–9143; (*e*) Y. Xie, T. T. Wang, X. H. Liu, K. Zou, X. H. Liu, K. Zou and W. Q. Deng, *Nat. Commun.*, 2013, **4**, 1960; (*f*) Y. Xie, T. T. Wang, R. X. Yang, N. Y. Huang, K. Zou and W. Q. Deng, *ChemSusChem*, 2014, **7**, 2110–2114; (*g*) Y. B. Zhou and Z. P. Zhan, *Chem. – Asian J.*, 2018, **13**, 9–19.

8 Y. Kou, Y. Xu, Z. Guo and D. Jiang, *Angew. Chem. Int. Ed.*, 2011, **50**, 8753–8757.

9 L. Chen, Y. Honsho, S. Seki and D. Jiang, *J. Am. Chem. Soc.*, 2010, **132**, 6742–6748.

10 J. Huve, A. Ryzhikov, H. Nouali, V. Lalia, G. Auged and T. J. Daou, *RSC Adv.*, 2018, **8**, 29248–29273.

11 M. H. Zeng, Q. X. Wang, Y. X. Tan, S. Hu, H. X. Zhao, L. S. Long and M. Kurmoo, *J. Am. Chem. Soc.*, 2010, **132**, 2561–2563.

12 A. Laybourn, R. Dawson, R. Clowes, T. Hasell, A. I. Cooper, Y. Z. Khimyak and D. J. Adams, *Polym. Chem.*, 2014, **5**, 6325–6333.

13 Y. Xu, S. Jin, H. Xu, A. Nagai and D. Jiang, *Chem. Soc. Rev.*, 2013, **42**, 8012–8031.

14 (*a*) J. X. Jiang, A. Trewin, D. J. Adams and A. I. Cooper, *Chem. Sci.*, 2011, **2**, 1777–1781; (*b*) H. Bohra, S. Y. Tan, J. Shao, C. Yang, A. Efrem, Y. Zhaob and M. Wang, *Polym. Chem.*, 2016, **7**, 6413–6421.

15 N. R. Kumar, P. Das, A. R. Agrawal, S. K. Mandal and S. S. Zade, *Mater. Adv.*, 2021, **2**, 7473–7481.

16 K. S. Song, P. W. Fritz and A. Coskun, *Chem. Soc. Rev.*, 2022, **51**, 9831–9852.

17 H. Gao, Q. Li and S. Ren, *Curr. Opin. Green Sustainable Chem.*, 2019, **16**, 33–38.

18 N. R. Kumar and A. R. Agrawal, *ChemOpen*, 2023, **1**, e202200203.

19 (*a*) S. B. Ren, W. Ma, C. Zhang, L. Chen, K. Wang, R. R. Li, M. Shen, D. M. Han, Y. Chen and J. X. Jiang, *ChemSusChem*, 2020, **13**, 2295–2302; (*b*) Z. Wang, J. Liu, Y. Fu, C. Liu, C. Pan, Z. Liu and G. Yu, *Chem. Commun.*, 2017, **53**, 4128–4131; (*c*) M. E. Bhosale, R. Illathvalappil, S. Kurungot and K. Krishnamoorthy, *Chem. Commun.*, 2016, **52**, 316–318; (*d*) W. Huang, J. Byun, I. Rçrich, C. Ramanan, P. W. M. Blom, H. Lu, D. Wang, L. C. Silva, R. Li, L. Wang, K. Landfester and K. A. I. Zhang, *Angew. Chem. Int. Ed.*, 2018, **57**, 8316–8320; (*e*) S. K. Kundu and A. Bhaumik, *ACS Sustainable Chem. Eng.*, 2016, **4**, 3697–3703; (*f*) S. K. Kundu, A. Kayet, R. Baidya, L. Satyanarayana and D. K. Maiti, *ACS Omega*, 2020, **5**, 394–405; (*g*) X. Liu, S. Wang, A. Wang, J. Chen, Z. Wang, Q. Zeng, W. Liu, Z. Li and L. Zhang, *J. Phys. Chem. C*, 2019, **123**, 21327–21335.

20 Q. Chen, M. Luo, P. Hammershoj, D. Zhou, Y. Han, B. W. Laursen, C. G. Yan and B. H. Han, *J. Am. Chem. Soc.*, 2012, **134**(14), 6084–6087.

21 (*a*) Y. He, Z. Guo, M. Chen, S. Wan, N. Peng, X. Fu, D. Yuan and B. Na, *J. Porous Mater.*, 2023, **30**, 1439–1448; (*b*) L. Zhang, H. Yu, W. Wu, Q. Ge, S. Ni, C. Song and K. Huang, *ChemNanoMat*, 2022, **8**, e202200215; (*c*) Y. Tao, H. Liu, H.-Y. Kong, T.-X. Wang, H. Sun, Y. J. Li, X. Ding, L. Sun and B.-H. Han, *Angew. Chem. Int. Ed.*, 2022, **61**, e202205796; (*d*) H. Wang, N. Qiu, X. Kong, Z. Hu, F. Zhong, Y. Li and H. Tan, *ACS Appl. Mater. Interfaces*, 2023, **15**(11), 14846–14853; (*e*) J. Yan, Y. Tan, L. Wei, Z. Liu, Q. Wang, H. Sun, Z. Wang, D. Li, Y. Qian and S. Guo, *Ind. Eng. Chem. Res.*, 2022, **61**, 13453–13460; (*f*) Q. Ge, H. Yu, L. Zhang, S. Ni, W. Wu, H. Yang, J. Liu and K. Huang, *Microporous Mesoporous Mater.*, 2022, **336**, 111865; (*g*) J. Yan, S. Tong, H. Sun and S. Guo, *Sep. Purif. Technol.*, 2023, **311**, 123205.

22 (*a*) Y. He, Z. Guo, M. Chen, S. Wan, N. Peng, X. Fu, D. Yuan and B. Na, *J. Porous Mater.*, 2023, **30**, 1439–1448; (*b*) S. H. Goudar, D. S. Ingle, R. Sahu, S. Kotha, S. K. Reddy, D. J. Babu and V. R. Kotagiri, *ACS. Appl. Polym. Mater.*, 2023, **5**, 2097–2104; (*c*) M. Zhang, Y. Du and H. Liu, *ACS Appl. Polym. Mater.*, 2023, **5**, 654–661; (*d*) N. Taheri, M. Dinari and M. Asgari, *ACS Appl. Polym. Mater.*, 2022, **4**, 6288–6302; (*e*) N. Das, R. Paul, D. Q. Dao, R. Chatterjee, K. Borah, S. C. Shit, A. Bhaumik and J. Mondal, *ACS Appl. Nano Mater.*, 2022, **5**, 5302–5315; (*f*) C. Li, H. Cai, X. Yang, F. Liu, C. Yang, P. Chen, Z. Chen and T. Zhao, *J. CO2. Util.*, 2022, **64**, 102203; (*g*) C. Yan, Y. Wu, H. Lu, H. Liu, G. Yi, M. Li, X. Cai, S. Gao and Z. Yang, *Z. Micropor. Mesopor. Mater.*, 2022, **343**, 112157; (*h*) J. Huang, C. Liu, Y. Jin and J. Chen, *Chem. Eng. J.*, 2023, **461**, 141930; (*i*) Y. Cao, Y. Wang, F. Zhou, J. Huang and M. Xu, *Sep. Purif. Technol.*, 2022, **303**, 122229; (*j*) N. Li, L. Huo, W. Shen, C. Qiang, M. Wu, G. Sun, Q. Li, M. Shi and J. Ma, *J. Cleaner Prod.*, 2023, **396**, 136558.

23 R. Maragani and R. Misra, *Tetrahedron Lett.*, 2013, **54**, 5399–5402.

24 Y. Luo, B. Li, W. Wang, K. Wu and B. Tan, *Adv. Mater.*, 2012, **24**, 5703.

25 Y. He, Q. Liu, F. Liu, C. Huang, C. Peng, Q. Yang, H. Wang, J. Hu and H. Liu, *Microporous Mesoporous Mater.*, 2016, **233**, 10–15.

26 (*a*) E. P. Barrett, L. G. Joyner and P. P. Halenda, *J. Am. Ceram. Soc.*, 1951, **73**, 373–380; (*b*) R. Jia, J. Chen, J. Zhao, J. Zheng, C. Song, L. Li and Z. Zhu, *J. Mater. Chem.*, 2010, **20**, 10829–10834; (*c*) H. Yang, S. Kannappan, A. S. Pandian, J.-H. Jang, Y. S. Lee and W. Lu, *J. Mater. Chem. A*, 2017, **5**, 23720–23726; (*d*) Y. Zhang, K. Zhang, L. Wu, K. Liu, R. Huang, Z. Long, M. Tong and G. Chen, *RSC Adv.*, 2020, **10**, 3606–3614.

27 A. Modak, Y. Maegawa, Y. Goto and S. Inagaki, *Polym. Chem.*, 2016, **7**, 1290–1296.

28 (*a*) P. Raveendran, Y. Ikushima, L. Scott and S. L. Wallen, *Acc. Chem. Res.*, 2005, **38**, 478–485; (*b*) L. Fu, Z. Ren, W. Si, Q. Ma, W. Huang, K. Liao, Z. Huang, Y. Wang, J. Li and P. Xu, *J. CO2 Util.*, 2022, **66**, 102260; (*c*) K. S. Song, P. W. Fritz and A. Coskun, *Chem. Soc. Rev.*, 2022, **51**, 9831–9852.

29 (*a*) S. Qiao, Z. Du and R. Yang, *J. Mater. Chem. A*, 2014, **2**, 1877–1885; (*b*) X. Zhu, S. M. Mahurin, S. H. An, C. L. Do-Thanh, C. Tian, Y. Li, L. W. Gill, E. W. Hagaman, Z. Bian, J. H. Zhou, J. Hu, H. Liu and S. Dai, *Chem. Commun.*, 2014, **50**, 7933–7936; (*c*) A. Palma-Cando, E. Preis and U. Scherf, *Macromolecules*, 2016, **49**, 8041–8047; (*d*) Y. Wei, W. Chen, X. Zhao, S. Ding, S. Han and L. Chen, *Polym. Chem.*, 2016, **7**, 3983–3988.

30 A. L. Myers and J. M. Prausnitz, *AIChE J.*, 1965, **11**, 121–127.

31 (*a*) X.-Y. Li, T.-Z. Li, Y. Yang, L. Hou, Y.-Y. Wang and Z. Zhu, *Chem. Commun.*, 2017, **53**, 12970–12973; (*b*) H.-Y. Yang, Y.-Z. Li, W.-J. Shi, L. Hou, Y.-Y. Wang and Z. Zhu, *Dalton Trans.*, 2017, **46**, 11722–11727.